DØNOTE 2908, May 7, 1996

# Determination of the Hadronic Energy Scale of DØ Calorimetry
(CAFIX version 5.0)

R. Kehoe,[1] R. Astur[2]

[1] *University of Notre Dame, Notre Dame, Indiana 46556*
[2] *State University of New York, Stony Brook, New York 11794*

## Abstract

The DØ calorimeter system is used to study jets produced in $\bar{p}p$ collisions and consists of central and forward liquid argon cryostats and scintillator calorimetry in the inter-cryostat region. Jets are reconstructed using fixed-cone and nearest neighbor clustering algorithms. The measured energy clustered is determined from a calibration obtained from a testbeam. Based on this energy, we want to determine the total energy of the matching jet reconstructed with this algorithm from the final state particles. This note describes the corrections applied, how they are obtained, and what their values are. The same methods applied to data are applied to parallel Monte Carlo samples giving us separate corrections for the real detector and the simulated detector. Verification proceeds by looking at $E_T$ balance in $Z + jets$ events, and by comparisons of Monte Carlo jets clustered before and after the calorimeter.

## Contents

## List of Figures

**List of Tables**

# I. INTRODUCTION

At a hadron collider the production of jets is copious and they are generally interpreted as the remnant of the partons participating in the hard scattering as shown in Figure 1a. The relationship between jets observed in the experiment and partons is most evident by looking at event displays where one observes localized depositions of energy which are easily recognized as jets. The fact that most events display a dijet structure intuitively connects the observed jets to an underlying simple parton interaction. Although this picture seems relatively straightforward, it is not easy to associate the jet energy with a specific underlying parton energy. The concept of an isolated parton simply does not exist in the theory of strong interactions (QCD). Partons fragment into hadrons and interact with one another via color flow. This complexity makes jet physics very dependent on the jet definition. There are numerous jet definitions; in DØ a fixed cone in $\eta - \phi$ space is most common [1], although nearest neighbor and successive combination clustering algorithms are also used. The fixed-cone algorithm itself has variations using cone-sizes ($\Delta R$) ranging from 0.3 thru 1.0.

The energy of jets is measured in central (CC) and forward (EC) liquid argon uranium calorimeters [2]. The transition region between these calorimeters is instrumented with scintillators and is referred to as the ICR ('inter-cryostat region'). Particles are not perfectly measured in a real calorimeter; hadrons suffer from non-linearities in low energy response, and all particles can deposit unmeasured energy in poorly instrumented regions of the detector. Also, as shown in Figure 1b hadrons in particular produce wide showers in the calorimeter. As a result, the measured jet energy, $E^{jet}_{measured}$, is skewed and jet physics becomes dependent on our ability to compensate for this.

For the purpose of this analysis, we define the true jet energy as the sum of all the final state particle energies contained in a fixed cone of size $\Delta R$ which matches a jet measured in the calorimeter with the same algorithm. We define this energy ($E^{jet}_{particle}$) to include only those particles arising from the partons participating in a hard scatter before any calorimeter effects due to showering or noise. The corrections that will be described do not attempt to correct back to the parton level. The energy assigned to a jet presupposes two things:

- A basic calibration of the calorimeter using testbeam data to obtain relative sampling weights and conversions for ADC counts to GeV [3,6].
- A precise *in situ* determination of the final electromagnetic energy scale using dielectron and diphoton decays of known resonances ($Z$, J/$\psi$ and $\pi^0$) [4,6,7]. This is the scale of electrons and photons in the best part of the detector. It is also valid for highly electromagnetic jets with shapes and characteristics similar to electrons or photons (ie. jets dominated by one $\pi^0$) [5,4].

Inherently tied up with the hadronic energy scale is our measurement of net transverse energy, the negative of which is the missing transverse energy ($\not\!\!E_T$) required in the event by energy conservation. In typical jet events without neutrinos in the final state, the average $\not\!\!E_T$ should be zero in a perfect detector. In a hermetic calorimeter such as DØ, $\not\!\!E_T$ is calculated as:

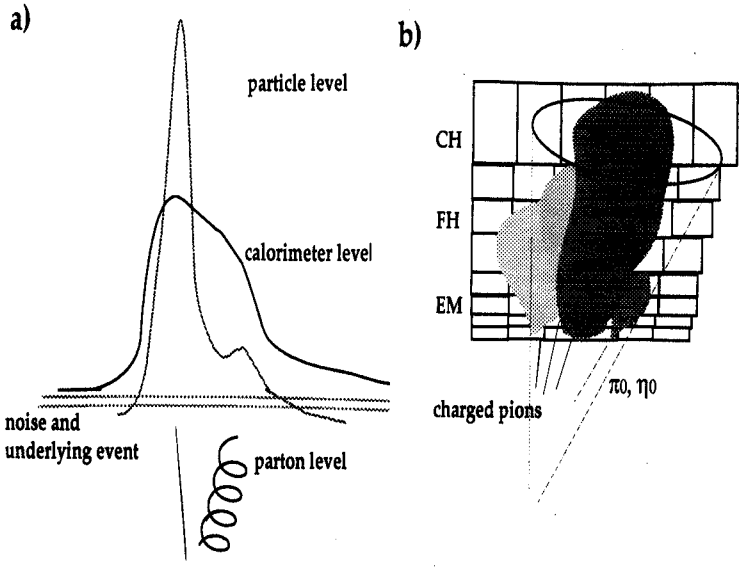


FIG. 1. a) Sketch of jets at parton, particle, and calorimeter levels. At the particle level, there is not a clear association of energy to each parton. At the calorimeter level, showering and noise further alter the energy profile. Sketch b) shows a section of calorimeter with individual particle showers. Charged hadrons, in particular, produce wide showers which can spill outside of a cone.

$$\not\!\!E_T = \sqrt{\not\!\!E_x{}^2 + \not\!\!E_y{}^2} \tag{1.1}$$

where

$$\not\!\!E_x = \Sigma_i E_i sin\theta_i cos\phi_i; \not\!\!E_y = \Sigma_i E_i sin\theta_i sin\phi_i \tag{1.2}$$

are summed over all calorimeter cells. In a calibrated detector with finite resolution, the average of this quantity projected onto any axis should be zero. We will use this fact in our attempts to measure jet response and to check the effectiveness of the overall correction.

When calculating $E^{jet}_{particle}$ from $E^{jet}_{measured}$, we must correct for the following effects:

I. those resulting in an overall change of the energy scale due to response, $R$, of the detector. This is ideally a jet-algorithm independent correction which when applied to all calorimeter energy is intended to balance the $\not\!\!E_T$ on average (see Section III).

   - jets typically consist of particles which span a wide range of energies. Non-linearities in the calorimeter result in a response dependence on jet energy. The non-linearities are of order 10% to 20% for charged pions below 10 GeV [5,6].
   - jets span large regions of the detector and cover cracks and uninstrumented regions [8].
   - overall scale difference of DØ detector components from those observed in corresponding testbeam modules. This includes possible scale variations between cryostats and would therefore have an $\eta$ dependence.

II. those which add/remove energy from the jet in a fairly constant fashion and typically depend on the cone-size.

- uranium noise leaves positive energy after zero-suppression.
- negative energy results from pile-up in a high instantaneous luminosity ($\mathcal{L}$) environment.

III. change in energy, $S$, due to showering in the calorimeter which is specific to each jet algorithm (see Section IV).

IV. particles from the underlying event are not considered part of the hard interaction. This includes particles from other interactions in the same bunch crossing.

Points II and IV are together combined in a total offset, $O$, and are described in Section II. The total correction can be summarized in the following way:

$$E^{jet}_{particle} = \frac{(E^{jet}_{measured} - O(\Delta R, \eta, \mathcal{L}))}{(1 - S(\Delta R, E, \eta))R(E, \eta, RMS_{\eta,\phi})} \tag{1.3}$$

where the jet angular width is denoted by $RMS_{\eta,\phi}$. This is defined as the sum in quadrature of the $\Delta\eta$ and $\Delta\phi$ root mean squared (RMS) values of cells in a jet relative to the jet centroid. Once $R$, $O$, and $S$ are known we can theoretically calculate $E^{jet}_{particle}$. While Equation 1.3 is simple enough, its implementaion requires a multi-step algorithm which is summarized in Section V.

Each step of our method involves assumptions and approximations which flaw the energy scale in a systematic way, and each method possesses a statistical limitation which may be significant. The philosophy in our determination of errors has been to attempt their estimation independently of our two major verification samples (Monte Carlo and Z events). This allows us to ascertain whether we agree with those samples within errors. Perhaps more importantly, it allows us to consider point-to-point correlations in these errors and their dependence on various variables. The total assigned errors are collected in Section V as well as a brief discussion of correlations.

Having estimated a correction and its potential error, we have verified it in four different comparisons:

- Response dependence on jet pseudorapidity and $RMS_{\eta,\phi}$ after corrections in terms of these variables.
- Response predicted by Monte Carlo versus that measured in DØ.
- $E_T$ of jets evaluated before calorimeter effects versus $E_T$ after (ie. $E^{jet}_{measured}/E^{jet}_{particle}$).
- transverse energy balance in $Z + jets$ events in Monte Carlo and collider data.

Our findings are documented in Section VI.

Finally, in Section VII we give our conclusions. For completeness, a skeleton description of the FORTRAN involved in correcting both jets and $\not\!\!E_T$ is given in Appendix C, as well as guidelines on proper manipulation of RCP files. This document is intended as a description of CAFIX V5.0. Very little mention is made of earlier incarnations of this analysis, the problems solved from earlier analyses, and the inevitable improvements for the future.

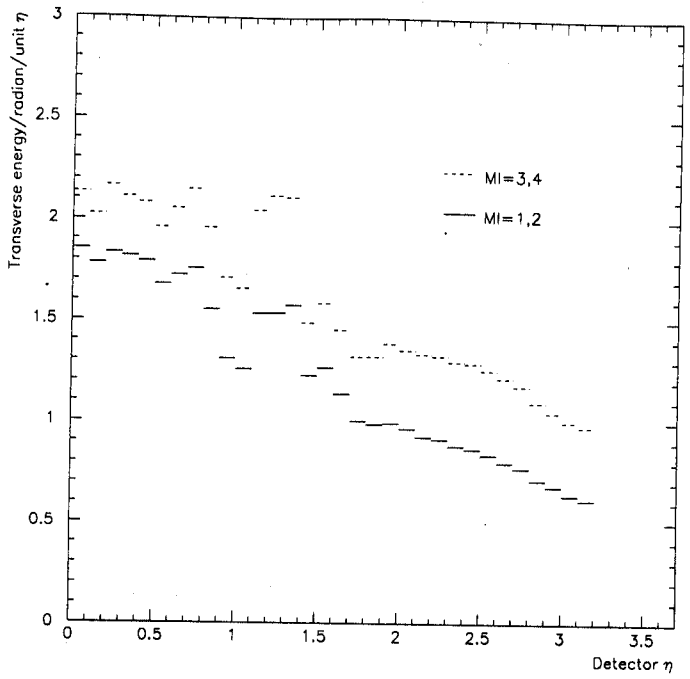


FIG. 2. Average $E_T$ density in GeV as a function of detector $\eta$, for both single interaction (MI=1,2) and two interaction (MI=3,4) candidate events.

## II. ESTIMATION OF OFFSET

Part of the measured jet energy does not originate from the particles making up the corresponding particle jet. Instead it arises from electronic noise, ionization caused by decay of uranium nuclei and other detector effects, labelled 'noise' and denoted $N$. Additional energy comes from beam remnants and additional 'spectator' $\overline{p}p$ interactions and is termed "underlying event" and denoted $U$. The total of these contributions gives the offset, $O$, in Equation 1.3.

Shown in Figure 2 is the average transverse energy ($E_T$) density in GeV/rad/$\eta$ as a function of detector pseudorapidity from a sample of events where particles between pseudorapidity of 1.7 and 3.0 are required on both sides of the interaction region (ie. MIN-BIAS trigger). We assume that both $U$ and $N$ are evenly distributed in $\phi$ and average the $E_T$ densities over all azimuth. The low curve is from events where only one interaction occurred in each event (Multiple Interaction Tool = 1,2). The second histogram was taken from events where at least one additional interaction occurred (Tool = 3,4). Based on the low $\mathcal{L}$ of the sample, we assume there was only one additional interaction.

The statistical error from using this sample is very small and is ignored. The systematic errors are derived from the differences in the results between the current numbers and those obtained with the last released version of the correction. For further discussion of systematics, see Appendix A.

### A. Underlying Event

One expects that the underlying event contribution for two interactions is twice that for single interactions. Thus, if $O$ is described accurately by the two histograms in Figure 2, the difference is a measurement of the underlying event contribution. We get:

$$U = O^{MI=3,4}_{MIN-BIAS} - O^{MI=1,2}_{MIN-BIAS} \tag{2.1}$$

This was fit as a function of detector $\eta$ with the result:

$$U = (0.310 + 0.034|\eta_d|)\ \mathrm{GeV}/rad/\eta \tag{2.2}$$

An excess of about 0.2 GeV/rad/$\eta$ shows up in the region $1.2 < |\eta| < 1.5$ (ICR) and is subtracted from jets piece-wise. The error on the underlying event $E_T$ density is 0.2 GeV/$rad/\eta$.

Because the number of extra interactions increases with $\mathcal{L}$, we need a luminosity dependent form for this correction. We can determine $U$ for each jet by multiplying the above density by the jet area in $\eta \times \phi$ space and by the number of extra interactions. By default, the number of extra interactions is calculated as [9]:

$$N_{interactions} = 0.1715 * \mathcal{L} \tag{2.3}$$

where $\mathcal{L}$ is in units of $10^{30}$. If this method is turned off, then the Multiple Interaction Tool is used to determine whether the event has one or two interactions. This method, however, cannot determine if more than one extra interaction is present.

### B. Noise

Since we have isolated the $U$ component in Equation 2.2, we can subtract it from the single interaction curve and the result is the noise contribution.

$$N = O^{MI=1,2}_{MIN-BIAS} - U \tag{2.4}$$

The result fits approximately to a sine curve with the result:

$$N = (0.196 + 1.44 sin\theta_d)\ \mathrm{GeV}/rad/\eta \tag{2.5}$$

Note that, unlike the underlying event, $N$ has no discontinuous step for the ICR. The error on $N$ in energy is 0.1 GeV/$rad/\eta$.

## III. RESPONSE

Once we have corrected the jet for the offset contribution, we are left with only that energy measured by the calorimeter due to the hard scatter. In the case of a jet, there is an effective global response to the energies of all hadrons, leptons, and photons produced by the fragmentation inside and outside a particular jet cone or nearest neighbor cluster. Several effects contribute to jet response being non-unity:

- Non-linear behavior of charged pions. This includes highly energetic pions which may be undermeasured due to punchthru. In testbeam, however, no evidence for this was seen in pion showers up to 150 GeV [5,6]. Using data and Monte Carlo, punchthru was measured to be small [10].
- Potential shifts in overall scale of each detector relative to testbeam. This includes the fact that jets are large objects which cover poorly instrumented regions not measured in the testbeam.
- Different response for the three cryostats and the ICR [11,4,12].
- Some jet energy lost to the zero-suppression cut.
- Inefficiency in reconstructing low $E_T$ jets results in biased response for jets found [13,18].
- Possible impurities or temperature variations in the liquid argon.

The response correction is factorized into three major components.

- Correct for cell level adjustments needed by different portions of the detector.
- Correct the jets for the dependence of their relative response on $RMS_{\eta,\phi}$.
- Bring jets up to an absolute calibration by correcting for the response variation vs. jet energy.

Without a magnetic field we cannot measure particle response *in situ*. We resort to $E_T$ balancing in dijet and direct photon candidates to determine the jet energy scale. Response results in measureable differences in cluster $E_T$'s when looking in dijet or direct photon events. Since there is alot of physics in direct $E_T$ balance which one would like to attempt to measure, we avoid using it to measure $R$. Response, however, also results in a measureable overall imbalance of transverse energy in the calorimeter and so contributes to $\not\!\!E_T$. Because little physics is involved in the calculation of $\not\!\!E_T$ besides conservation of energy, we rely on the $\not\!\!E_T$ to measure $R$ and elevate the so-called 'MPF' (Missing $E_T$ Projection Fraction) method [14] to this role. This has required more sophistication in its application and we summarize the important issues below.

In general we look in dijet events as shown in Figure 3 to determine the response relative to a 'trigger' jet which must pass a single jet trigger. With this requirement, the other 'probe' jet is unbiased. In order to obtain the response of the probe jet in terms of the $\not\!\!E_T$ let us consider a general event with the three vectors: $\vec{E}_T^{\,trigger}$, $\vec{E}_T^{\,had}$, and $\vec{E}_T^{\,\nu}$. $\vec{E}_T^{\,had}$ is the vector sum of all interacting particles in the event outside of the trigger jet ($= \vec{E}_T^{\,probe} + \vec{E}_T^{\,jet2}$ of Figure 3b), and $\vec{E}_T^{\,\nu}$ is the vector sum of all non-interacting particles in the event (ie. neutrinos). In the transverse plane at the particle level we have

$$\vec{E}_T^{\,trigger} + \vec{E}_T^{\,had} + \vec{E}_T^{\,\nu} = 0. \tag{3.1}$$

If $\vec{E}_T^{\,\nu}$ is negligible, this reduces to

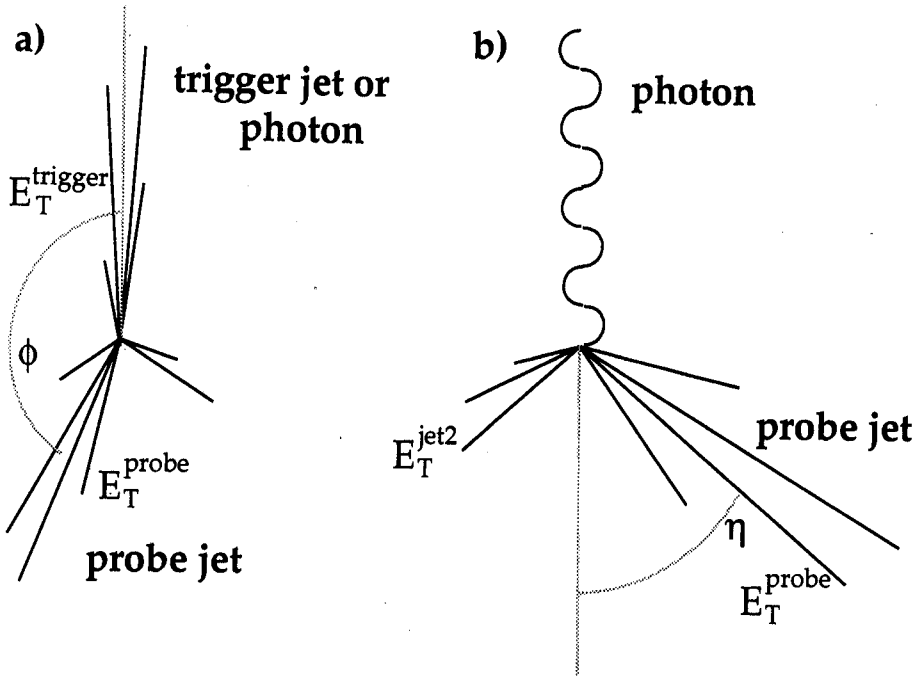


FIG. 3. Sketch of the $\not\!\!E_T$ Projection Fraction (MPF) method showing the trigger jet and the recoiling hadronic system. Dijet events, shown in a), are required to have only two jets for relative measurements. Photon plus jets events, shown in b), are left unbiased and are used to absolutely calibrate jets.

$$R^{trigger}\vec{E_T}^{\,trigger} + R^{had}\vec{E_T}^{\,had} = -\vec{\not\!\!E}_T \tag{3.2}$$

at the calorimeter level. As a specific example, let us consider events where the trigger jet is a photon with $R^{trigger} = 1.0$ and $\vec{E_T}^{\,trigger} = -\vec{E_T}^{\,had}$. Multiplying by $\vec{E_T}^{\,trigger}$ and equation 3.2 reduces to

$$(E_T{}^{trigger})^2 - R^{had}(E_T{}^{trigger})^2 = -\vec{\not\!\!E}_T \cdot \vec{E_T}^{\,trigger}. \tag{3.3}$$

From this we obtain the response of the hadronic recoil as:

$$R^{had} = 1 + \frac{\vec{\not\!\!E}_T \cdot \hat{n_T}^{trigger}}{E_T{}^{trigger}} \tag{3.4}$$

This quantity only involves the $\not\!\!E_T$ and the trigger jet, and in an event with only two particle level jets and no offset or showering, it becomes $E_T{}^{jet}_{measured}/E_T{}^{jet}_{particle}$. In a situation where $E_T{}^{jet2} > 0$, Equation 3.4 is an approximation we use to get the response of the probe jet, $R^{probe}$. The discrepancy is small, however, and we can plot $R$ in terms of any property, $X$, of the probe jet. It is possible 'jet2' is some unreconstructed soft recoil energy with a finite response. Ideally this unclustered energy should also be corrected for a proper $\not\!\!E_T$ measurement and an attempt to do so is mentioned in Section III F.

We use two samples of data: QCD dijets, and direct photon candidate events. For the relative calibrations in terms of well-measured quantities (eg. $\eta$, $RMS_{\eta,\phi}$), we determine the correction using events with only two reconstructed jets so that we can assume the measured response variations are due mostly to the probe jet. The event must pass QCD inclusive triggers requiring a central ($\eta < 0.7$) jet above 20, 30, 50, 85, or 115 GeV. The $\not\!\!E_T$ is biased

by our cuts on the trigger jet and 'jet2', and this contributes to an overall normalization in measured $R$. Since we only care about the relative dependence of $R$ on $X$, we observe this bias and normalize it away. We assume that the bias is independent of the properties of the probe jet we wish to measure.

In the much smaller sample of events with one highly electromagnetic jet ('photon'), one can obtain an absolute response for the probe jet because the trigger jet (the photon) is absolutely calibrated. In addition, the excellent energy resolution of the photon allows us to make a calibration in terms of poorly measured properties such as jet energy or $E_T$. If $X$ has a poor resolution the measurement of response in terms of $X$ is biased. Studies indicated that, if $X = E^{jet}_{measured}$ or $E^{jet}_T$ for instance, even simple input response functions could not be determined [13]. However, both the $E_T$ of the photon and the direction of the probe jet are well-measured so we define the quantity, $E'$:

$$E' = E^{\gamma}_T cosh(\eta_{jet}) \tag{3.5}$$

In events with two particle jets, $E' = E^{jet}_{particle}$ and even in multijet events it is highly correlated with jet energy. We can now determine the proper dependence of response on energy by plotting $R$ vs $E'$. We note that $E'$ is fairly independent of the jet algorithm. Due to these features, we will use this quantity for the different photon analyses below.

In the photon analyses, we use triggers in Run 1a and 1b which required one isolated L2 electromagnetic cluster with shower shape consistent with a photon and thresholds ranging from 6, thru 40 GeV. Offline, we select direct photon candidate events where the photon satisfies photon quality cuts to remove major backgrounds. These include cuts on EM-fraction and isolation (eg. $> 0.96, < 0.15$ at 30 GeV, respectively) to remove EM jets with significant associated hadronic activity. They also include cuts on EM-clusters with a track in a road to the vertex to remove Drell-Yan backgrounds. As an example, these cuts are trackmatch significance $> 3.0$, $dE/dx < 0.6$ or $dE/dx > 1.5$, and TRD $\epsilon_T < 0.1$ or $\epsilon_T > 0.9$ for events with 30 GeV EM clusters. We do not cut on ${E_T}^{jet2}$ so a systematic error is estimated using Monte Carlo (see below).

### A. Removal of Electromagnetic Clusters from Jets

As stated in the Introduction, DØ has a precise calibration of electromagnetic objects. While it has been shown that this does not mean jet energy in EM compartments necessarily adheres to this scale [16], we can apply it to reconstructed non-isolated electromagnetic clusters found within jets [17]. Details of the EM calibration are presented elsewhere [4,6,7]; we merely note here that all reconstructed EM clusters are corrected by this scale and considered fully calibrated. We propagate these corrections into the $\not\!\!E_T$. For the purposes of jet correction we remove such clusters from jets vectorially, correct what remains as a normal jet, and then add the EM clusters back into the jet.

### B. Low $E_T$ Reconstruction Bias

Since the reconstruction procedure for jets requires the $E_T$ of the jet to be above 8.0 GeV (5.0 GeV for nearest neighbor jets), hadronic energy resolution produces an $E_T$ bias

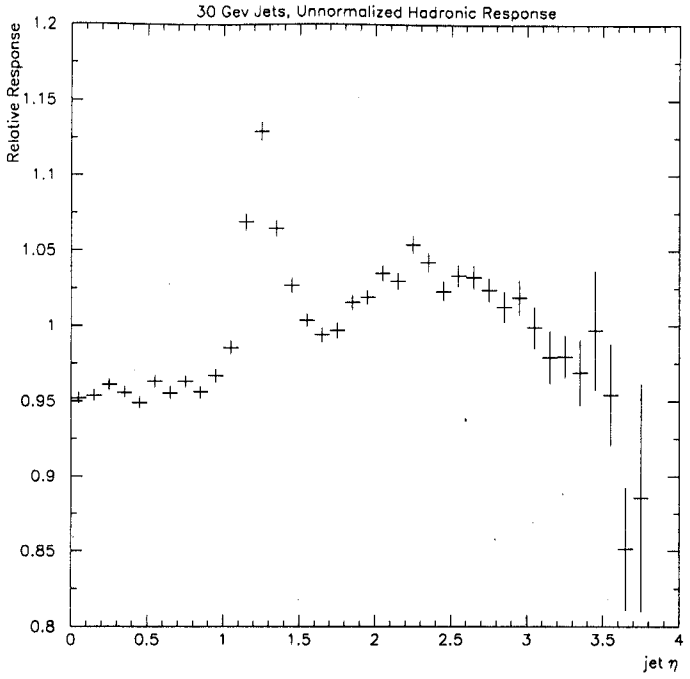


FIG. 4. Relative hadronic response as a function of jet pseudorapidity in dijet events where the trigger jet is over 30 GeV in $E_T$. The ICR jets have much higher response than central jets.

near this cutoff. Because this bias is a matter of resolution and not response, we do not always wish to correct for it, but we do want to 'unbias' the absolute scale measurement which is determined later. We measure this bias by plotting the response as calculated in Equation 3.4 vs photon $E_T$ in photon events with and without requiring a jet. Dividing the plot with the jet required by the plot with no such requirement gives the bias vs the photon $E_T$. After the division, the photon $E_T$ on the $x$-axis is scaled to the average jet $E_T$ giving us a measure of the bias vs jet $E_T$. Energy scale variations between cryostats and degradation in $\not\!\!E_T$ resolution with increased numbers of multiple interactions mean that this approach breaks down in the data because the two histograms we are dividing have more differences than just the requirement of a jet [18]. We have generated a sample of ISAJET [19] direct photon events which does not suffer from these problems because the recoil was specified to be central at generation time and the sample is all single interactions [18]. Because this bias is relative to the uncorrected $E_T$ threshold of 8.0 GeV (or 5.0 GeV for nearest neighbor jets) this correction is applied before any other jet corrections except for the EM-cluster removal mentioned above. It does have a systematic error due to the fact that the final bins are finite in size and the correction is steeply changing as a function of jet $E_T$ and this is given in Table III.

### C. Relative Detector Scales

Given the fact that four different devices make up the DØ calorimeter system (CC, ECS, ECN, ICR), we must determine any scale variations between them. This includes well known

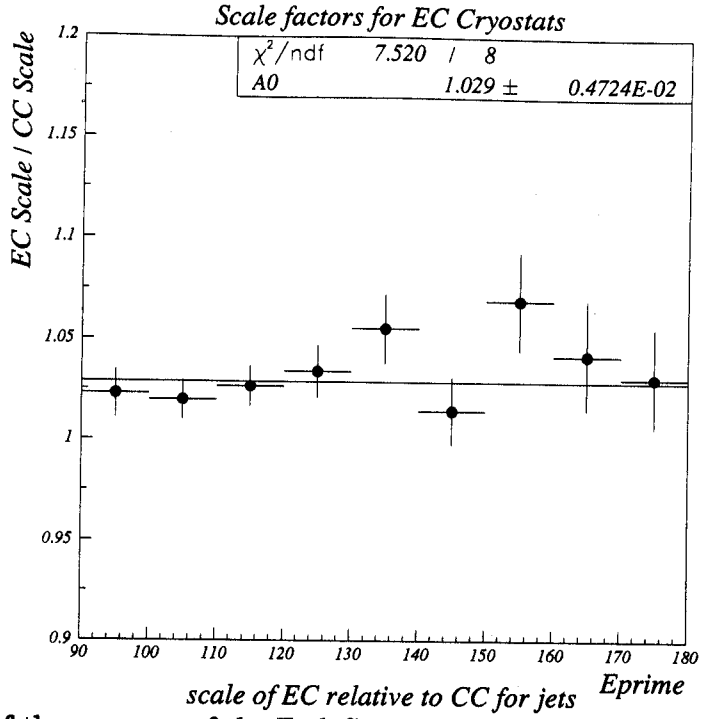


FIG. 5. Ratio of the response of the End Cryostats compared to that of the Central Cryostat in direct photon candidate events.

sampling weight changes and other less precise adjustments. Two cell-level corrections (ICR, EC) were determined at least in part using the MPF method and will be discussed below. For the high voltage adjustments needed for DØRECO version 10, we use the standard factors [12] given in Table IV for reference. For the sampling weight changes implemented in going from DØRECO version 11 to version 12, we use the numbers given in Table V. Additional details on the detector scale corrections are given in Appendix B.

The variation in relative jet response as a function of pseudorapidity of the probe jet is shown in Figure 4 for RECO 11 in dijet events. Here, the dependence is measured for 0.7 cone probe jets in events with the trigger jet above 30 GeV in $E_T$; the mean probe jet $E_T$ is 31.7 GeV for this sample. As one can see, there is a large increase in measured response in the ICR which is a well-known problem with ICR sampling weights for older reconstruction versions. In order to correct for this, sampling weights derived by the ICR group [11] were applied to the ICR jets. A reanalysis of dijet events using the MPF method showed that these sampling weights were not sufficient to correct the ICR bump (see Appendix B) and so additional adjustments dependent on both $E_T$ and $\eta$ were determined from the dijet sample.

It also appears that there is about a 3% higher response in the EC relative to the CC although one should remember that the energies (and thus the responses) are higher in the EC. In order to ascertain the scale factor between EC and CC as a function of energy, we resort to the photon sample. We use $E'$ because it is algorithm independent and because it is not subject to the $\eta$-dependent changes in showering and offset which have nothing to do with response. We plot $R$ vs $E'$ in CC and EC separately and take the ratio where they overlap as in Figure 5. It is consistent with a flat scale factor ($\chi^2 = 7.5$ for ndf=8)

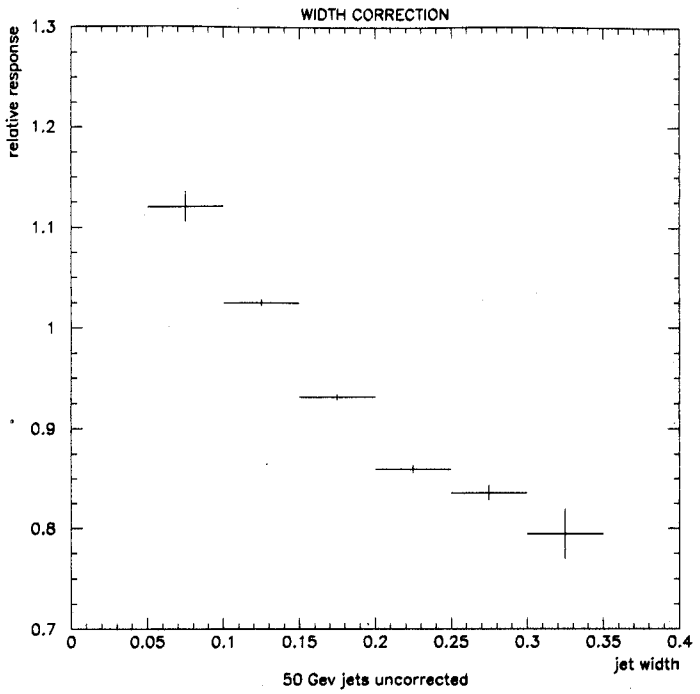


FIG. 6. Relative hadronic response in dijet events as a function of probe jet angular width. Narrow jets have a higher response than wide jets.

of $1.029 \pm 0.005$ and no offset. The ratio of response for ECN/ECS is about 1.1%. The EC/CC ratio is consistent with the ratio obtained using electrons from $Z$ decays, although a smaller difference between ECN and ECS is seen for jets. Because of this, we currently use the MPF measurement for the cryostat corrections for jets. This ratio is sensitive to the number of multiple interactions in an event and this results in a 2% systematic error [18]. Also, while the energy of the probe jet is high, the $E_T$ of the photon used for this study is relatively low so that we must apply a small systematic error due to initial state radiation going down the beampipe. This is given in Table III.

### D. Response Dependence on Angular Width of a Jet

It has been shown that jets have higher response not because they showered in the EM section but because they fragmented into fewer particles [16]. Thus one might expect jet response to depend on $RMS_{\eta,\phi}$. We define the relative response as in Equation 3.4 and plot the measured response as a function of the $RMS_{\eta,\phi}$ of the probe jet in dijet events as in Figure 6. This is done for probe jets in two regions: central ($\eta < 0.7$) and forward ($\eta > 1.7$). The ICR was avoided due to the non-uniformities in this region. The curves show a very strong dependence on jet width with wide jets having lower response than narrow jets. Further, the dependence of relative response on the width decreases with both probe jet pseudorapidity and $E_T$. Interpolation is done between $E_T$ regions and the forward jet results are used in the ICR as well even though the jet width is not well-measured there. No error is assigned to this correction because the various curves are fit and normalized by the

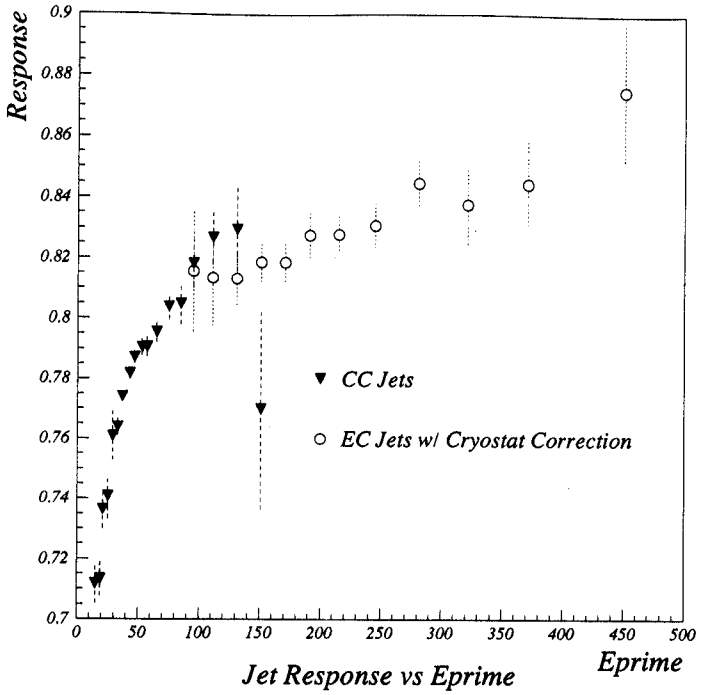


FIG. 7. Hadronic response of the calorimeter versus the $E'$ in direct photon candidates. Solid triangles are central cryostat data; open circles are end cryostat data.

average response. This results in a correction which on average should not change the overall jet response. Even if it shifts the energy scale of jets, the absolute scale correction which is determined afterwards will correct for it as long as there are photon events to register the effect.

### E. Absolute Hadronic Scale

Once the above corrections have been applied, it remains to anchor the jet to an absolute energy scale. We wish to measure the absolute response in terms of the measured jet energy since that is the independent variable in low energy pion non-linearities from testbeam studies. A full treatment can be found in [18].

We use Equation 3.4 to give us a histogram of the absolute response as a function of $E'$ (see Figure 7). This is, however, not directly applicable to determining the correction for a jet in a general event where we only know $E^{jet}_{measured}$. In order to relate the response to the measured jet, we measure the average jet energy also as a function of $E'$. This results in a second histogram (Figure 8) which can be combined with Figure 7 to give the average response as a function of average jet energy. It should be noted that this correction does not in any way force the probe jet to directly balance the trigger jet or equal $E'$. This procedure worked almost perfectly in toy Monte Carlo simulations with effects such as jet resolution, photon resolution, falling cross section, and RECO thresholds simulated [13].

The above method for determining a jet's response possesses several systematics which include the effects of initial or final state radiation, resolution bias, binning, and unbiasing low energy jets. For situations in a secondary jet is present and hits the calorimeter, Equation 3.4 is an approximation. This 'topological' error is found by measuring the response

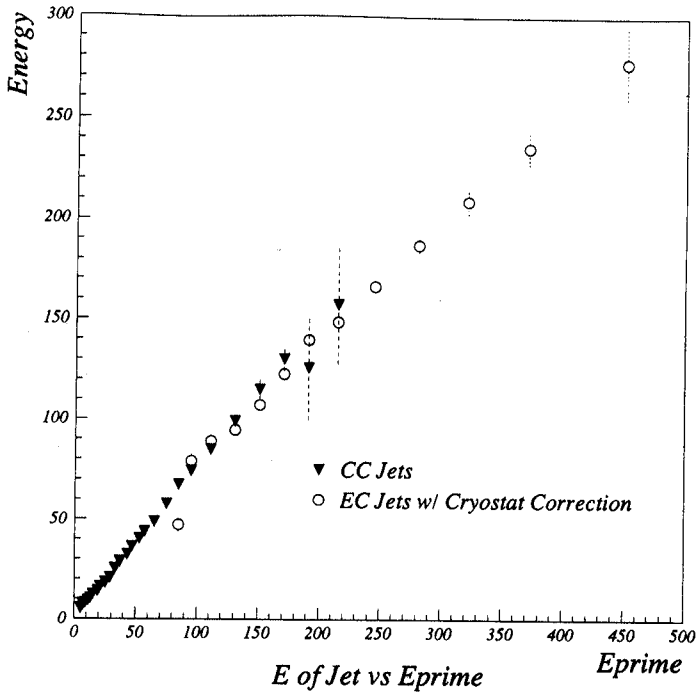


FIG. 8. Correlation between the jet energy and $E'$ in direct photon candidates. Solid triangles are central cryostat data; open circles are end cryostat data.

in ISAJET direct photon events generated with only one central jet and processed thru showerlibrary, and comparing with ISAJET showerlibrary events in the same energy region which had no jet cuts. The error ranges from 1% to 2% depending on jet energy and is given in Tables I and II. Another problem is due to initial state radiation which is lost down the beampipe. From toy Monte Carlo studies, the estimated deviation is about 2% for events with low $E_T$ photons (ie. less than 30 GeV) [18]. The binning systematic comes from the finite size of bins in our final response vs jet energy plots. This error is the change in response over the binsize in this region.

Backgrounds to direct photons are a source of error for this analysis, particularly in collider data. Our instrumental background is estimated by comparing the measured response in events with photon candidates having or lacking a track in a road to the vertex after applying quality cuts. The physics background consists of various Drell-Yan signals and diphoton production left after cuts designed to reduce them. In collider data, the major problem comes from W plus jet events which are removed by a loose $\not\!\!E_T$ cut and the tracking quality cuts mentioned above.

Because the energy reach from central jets is limited to $< 150$ GeV, we need to extrapolate our scale. It is common for more than half of the jet's energy to be carried by particles with less than a tenth of the total energy. Since the electron/pion response ratio is not unity and decreases with energy, we expect a rise in response with energy but the cumulative response to be below 1.0 even for high energy jets. One may also consider that there is a logarithmic energy dependence of the fraction of a hadronic shower which results in $\pi^0$'s [20] and hence electromagnetic energy. Also, the effect of dead material will be fairly energy independent and reduce jet response below 1.0 [8]. As a result, Monte Carlo and testbeam suggest that a flattening out of R vs jet energy occurs and that in fact appears in Figure 7.

TABLE I. Collider Data Jet Response Errors (augmented by MC) given in % ($\delta R/R$) for seven energy points. The lines marked *** are the errors on the cryostat factors and are applied only for CC jets. The line marked ** is the error in unbiasing and is only applied if the bias correction is turned off. The row labelled '$k_T$/res-bias' refers to initial state radiation passing down the beampipe as well as the minor effect due to a residual resolution bias.

| Source of Error | 10 GeV | 15 GeV | 20 GeV | 30 GeV | 80 GeV | 150 GeV | 400 GeV |
|---|---|---|---|---|---|---|---|
| statistical: | | | | | | | |
| method: | | | | | | | |
| topology | 0.0 | 0.0 | 2.02 | 1.78 | 1.22 | 0.88 | 0.88 |
| $k_T$/res-bias | 2.0 | 1.0 | 3.0 | 1.0 | 0.0 | (1.0)*** | 1.0 |
| binning | 1.0 | 1.0 | 0.0 | 0.0 | 0.0 | 0.0 | 0.0 |
| unbiasing** | 5.0 | 0.5 | 0.0 | 0.0 | 0.0 | 0.0 | 0.0 |
| background: | | | | | | | |
| instrumental | 0.0 | 0.0 | 1.73 | 1.42 | 1.42 | 1.42 | 0.0 |
| physics | 0.5 | 0.5 | 0.5 | 0.5 | 0.5 | 0.5 | 0.5 |
| mult-interactions | 0.0 | 0.0 | 0.5 | 0.5 | 0.5 | (2.0)*** | 0.0 |
| MC-data conversion | 3.20 | 3.20 | 0.0 | 0.0 | 0.0 | 0.0 | 3.71 |

Unfortunately, we cannot tell from CC jets alone how much it is flattening. We include EC jets after cryostat corrections, therefore, to establish this.

A full analysis of the Monte Carlo using the same techniques has a similar functional form but the level is a few percent higher. The ratio of the two data sets is shown in Figure 9. Over the range 30 to 350 GeV the ratio is flat ($\chi^2 = 9.9$ for ndf=12) at $1.075 \pm 0.003$. The collider data curve for jet energies below 15 GeV is not reliable and we have no data above 350 GeV. These energies are important to many physics analyses so we do not resort to a blind extrapolation. Instead we normalize the Monte Carlo curve by 1/1.075 and use it for jets below 25 GeV and above 350 GeV. We must also redefine the errors here. For instance, there is no instrumental background in the Monte Carlo but the effect of this is in the Monte Carlo/data ratio used to renormalize the Monte Carlo curves to the data. Thus, certain errors drop out but some are part of an overall Monte Carlo to data error which is about 3.5% (see Table I). This number is obtained by adding in quadrature the errors that are different between Monte Carlo and Collider Data at 20 GeV and at 350 GeV (the extremes of the data plots). These errors are: secondary jets, energy lost down beampipe, resolution-bias, instrumental background, and multiple-interaction dependence.

The dependence on $E$ is well fit by the form:

$$R = a + b \cdot ln(E_{jet}). \tag{3.6}$$

For data, $a = 0.71, b = 0.025$, for Monte Carlo, $a = 0.74, b = 0.031$. The shapes of the Monte Carlo and data in these two fits do not reflect the 7.5% scale factor seen in the MC/data ratio mentioned above. This is because the RMS correction, which was derived from the data and applied to the Monte Carlo, biases the Monte Carlo which has significantly narrower jets

TABLE II. Monte Carlo Jet Response Errors given in % ($\delta R/R$) for seven energy points. The line marked ** is the error in unbiasing and is only applied if the bias correction is turned off. The row labelled '$k_T$/res-bias' refers to initial state radiation passing down the beampipe as well as the minor effect due to a residual resolution bias.

| Source of Error | 10 GeV | 15 GeV | 20 GeV | 30 GeV | 80 GeV | 150 GeV | 400 GeV |
|---|---|---|---|---|---|---|---|
| statistical: | | | | | | | |
| method: | | | | | | | |
| topology | 0.0 | 0.0 | 0.0 | 0.0 | 0.0 | 0.88 | 0.88 |
| $k_T$/res-bias | 2.0 | 1.0 | 1.0 | 0.0 | 0.0 | 0.0 | 1.0 |
| binning | 1.0 | 1.0 | 0.0 | 0.0 | 0.0 | 0.0 | 0.0 |
| unbiasing** | 5.0 | 0.5 | 0.0 | 0.0 | 0.0 | 0.0 | 0.0 |
| background: | | | | | | | |
| instrumental | 0.0 | 0.0 | 0.0 | 0.0 | 0.0 | 0.0 | 0.0 |
| physics | 0.5 | 0.5 | 0.5 | 0.0 | 0.0 | 0.0 | 0.5 |

than the data. The MC/data scale factor was derived with the RMS correction turned off.

Table I contains a re-iteration of the errors on the Collider Data response correction. Table II gives the corresponding errors for the Monte Carlo response correction.

### F. $\not\!\!E_T$ Correction and Soft Recoil

Since we have changed the energy scale of the objects in an event, we will have to adjust the $\not\!\!E_T$ by these changes. We assume for now that $O$ has no $\phi$ dependence and since the $\not\!\!E_T$ is summed over all cells in a calorimeter system which has full $2\pi$ azimuthal coverage, this term is not needed for determining $\not\!\!E_T$. Since $S$ describes energy lost by the algorithm but not by the calorimeter, it also is not used for $\not\!\!E_T$. (Actually, there is a term $S(1-R)$ which should go into the $\not\!\!E_T$ but we ignore it.) The $\not\!\!E_T$ is thus only adjusted by the response corrections for jets and electrons. The only portion of the $\not\!\!E_T$ that is still not corrected is that due to the response of soft energy which is in the calorimeter but not contained in any found object. Such a correction was obtained by looking at $R$ measured according to Equation 3.4 in Z dielectron events where no jets were reconstructed. In this case, ${E_T}^{trigger} = p_T^Z$. Preliminary studies question the usefulness of this correction, however, because the gains are small and because such corrections amplify the noise as well as the signal and they are of comparable size [21]. Currently the default is for this soft recoil correction to be turned off.

## IV. SHOWERING

Up to this point we have discussed algorithm independent corrections. Now we delve into the correction which is algorithm specific and whose purpose is to adjust for losses by the algorithm due to hadron showering. We define that there is no correction needed for the

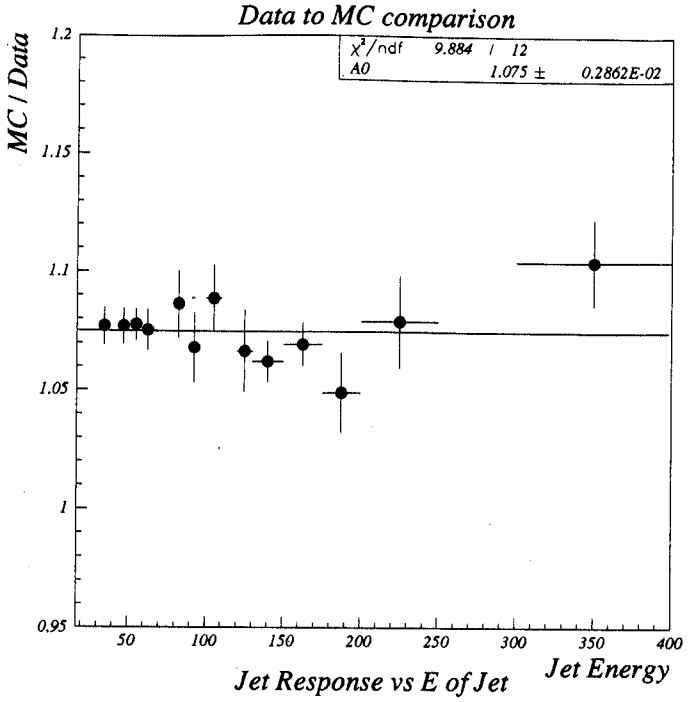


FIG. 9. Ratio of responses for Data and Monte Carlo using direct photon candidates. It is consistent with a scale factor of 1.075 with no offset.

algorithm when it is applied at the particle level. Gluon radiation and parton fragmentation can also result in energy lost outside of a jet, but the treatment of this energy is of physics interest so we only correct for the detector-based showering losses for the fixed-cone jets.

### A. Central Region

Central jets ($\eta < 0.7$) are generated with HERWIG [22] at various energies. In step 1, the hadrons/photons that make up this jet are replaced with randomly chosen testbeam Load II pions/electrons of similar energy. Since these particles are measured after zero suppression, some noise will be present in these testbeam showers. A scale factor is applied to move the beam momentum of the testbeam particle to the energy of the HERWIG particle. In this step, all of the energy of this particle is deposited in the first calorimeter cell intercepted by its momentum vector. The cone jet finder is then applied and a list of resulting 'unshowered' jets obtained.

In step 2, the same thing is done, but instead of depositing all of the particle's energy in one place, it is distributed relative to the intercepted cell in the same way it was measured in Load II relative to the bench mark point. The jet finder is run again and a list of resulting 'showered' jets is obtained. The showered and unshowered jets are matched and the average ratio of showered energy to unshowered energy is plotted as a function of the energy of the incident particle jet energy. Since we are only calculating the fraction of energy lost, we expect that the noise contributions cancel out to some extent. For $\Delta R = 0.7$, the ratio

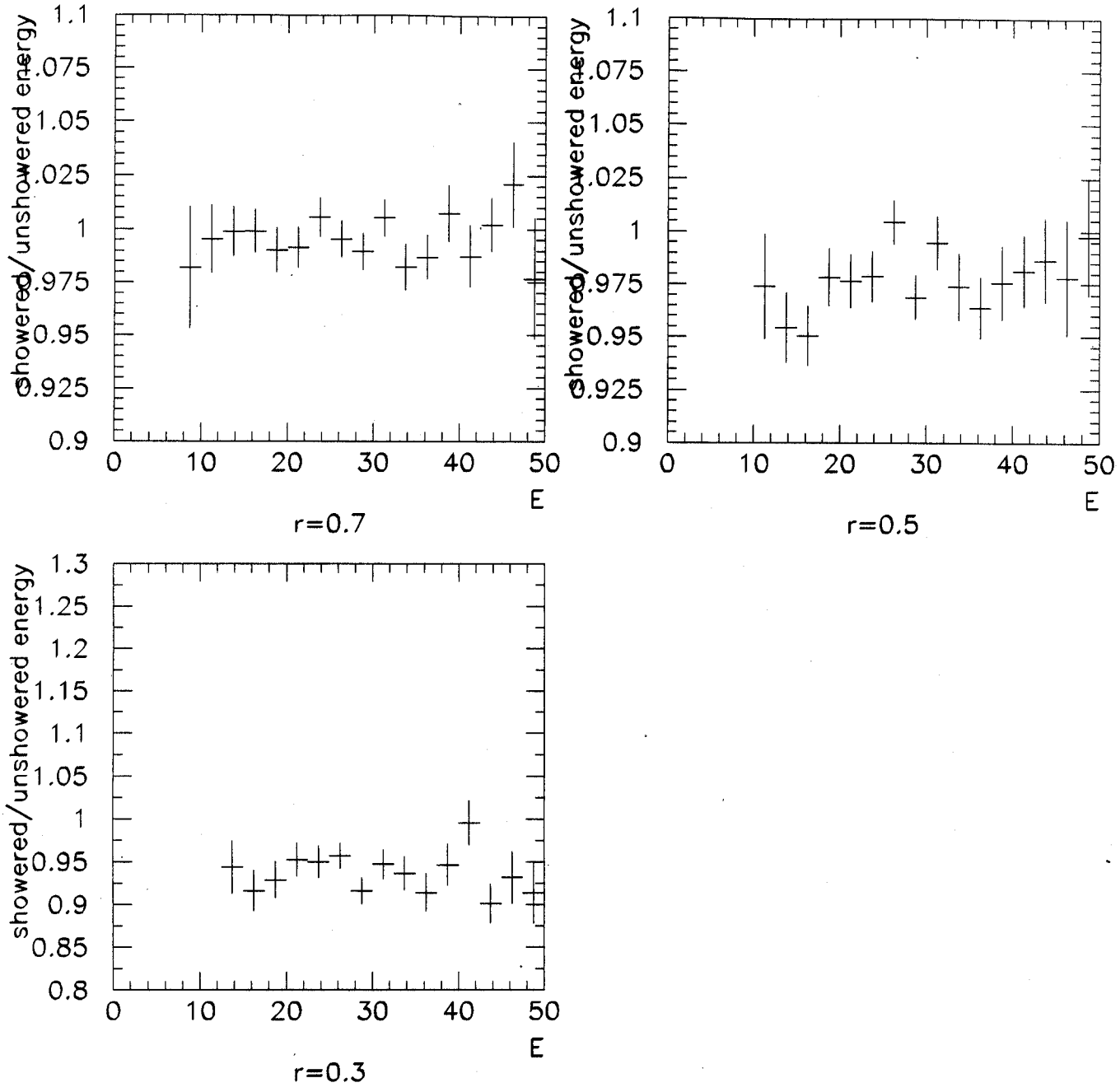


FIG. 10. Ratio of showered and unshowered jets for cone-sizes of 0.7, 0.5, and 0.3 in $\eta - \phi$ after removing response effects.

$(= 1 - S)$ is 0.99 to 1.01. For $\Delta R = 0.5$, the shower losses start near 0.97 and rise slowly to 1.00. For $\Delta R = 0.3$, the curve starts near 0.94 and again rises slowly. The behavior of these three cone-sizes for jets below 50 GeV is shown in Figure 10. For $\Delta R = 1.0$, the curve was identically 1.0, partly because the HERWIG jet input was found with a cone of $\Delta R = 1.0$, so there is no possibility of 'outside' energy coming back into the cone. However, it IS important that for this cone-size no significant amount of energy left the cone.

The nearest neighbor algorithm presents a difficulty in that such jets have no readily defined boundary making showering losses difficult to assign. The approach taken here was to lump fragmentation, gluon radiation, and showering together for such clusters. At the particle level, a 1.0 cone jet was clustered. Then reconstructed nearest neighbor jets within 1.0 in $\eta - \phi$ of the centroid were matched to it. The algorithm correction was then taken to be the difference between the particle jet and the sum of the nearest neighbor jets. This difference was divided among the nearest neighbor jets according to the fraction of the total energy they already had. Although this has the benefit of putting almost all unreconstructed energy into reconstructed jets, it places the nearest neighbor on a fundamentally different footing than fixed-cone jets.

The measured value of $S$ for high energy 0.7 cone-size jets indicates a net showering of energy into the cone, rather than out. Until this effect is understood better, we do not remove this energy but assign a systematic error of 1.0% for all algorithms, energies, and pseudorapidities.

### B. Forward Region

Our method assumes that the pion shower at the Load II bench mark point can be applied equally anywhere in the central calorimeter. This limitation prevents us from obtaining algorithm corrections in the ICR and forward regions. At one time, explicit dijet balance as a function of $\eta$ was used to determine the sum of both the jet response and the algorithm losses as a function of $\eta$. However, it was pointed out that increased soft radiation as one jet moves forward complicates the measurement and cannot be compensated for without using a QCD prediction (and thus preventing a measurement of this). Thus, we resort to an explicit calculation which considers that the jet shower does not get boosted as the jet moves forward (ie. size in $\theta - \phi$ constant), thereby expanding in $\eta$.

## V. CORRECTION ALGORITHM AND ERRORS

A brief description of the steps taken in the correction follows:

- In data only, correct all electromagnetic clusters with the EM-scale regardless of whether they are inside or outside of jets. In Monte Carlo, the same is done but the EM energy scale was assumed to be 1.0.
- Remove any reconstructed electromagnetic clusters from jets. The remaining energy, if significant (above 4 - 8 GeV), will be corrected as a jet.
- If no electromagnetic clusters are removed apply low $E_T$ bias correction (if turned on).

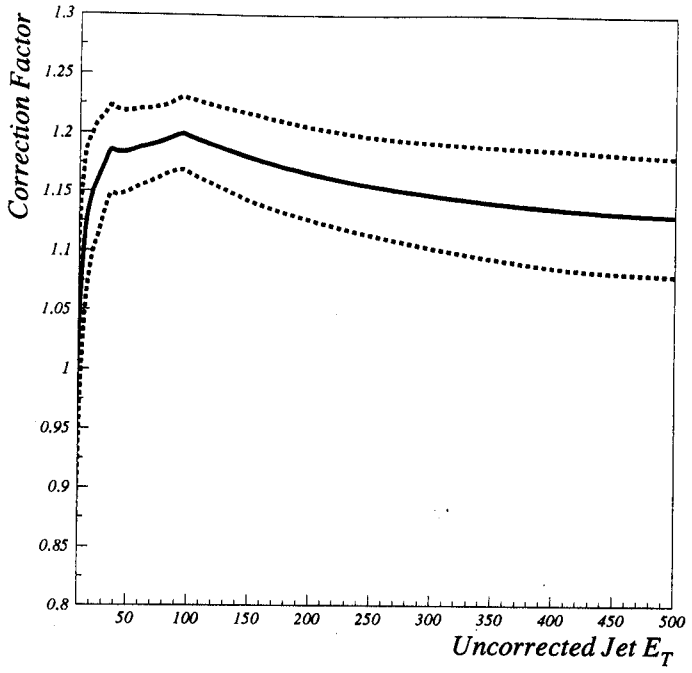


FIG. 11. Correction Factor applied in the Inclusive Jet Cross Section analysis. The average jet width as a function of jet $E_T$ was fit out to 300 GeV and this parametrization was used to estimate the overall correction.

- Remove the noise and underlying event from the jet.
- In data only, apply various relative detector scale corrections to jet.
- Correct jet for $RMS_{\eta,\phi}$ dependence of response.
- Apply absolute hadronic scale calibration.
- Correct for showering effects.

At this point, the jets of all algorithms have been corrected and it remains to correct the $\not\!\!E_T$:

- All response corrections for 0.7 cone jets are propagated into the $\not\!\!E_T$.
- All good muons are added vectorially into muon-included $\not\!\!E_T$. It should be noted that no effort to deal with the minimum ionizing energy left by the muon in the calorimeter is attempted.
- Soft recoil response is also added into $\not\!\!E_T$ (if requested).

The cumulative correction used in the analysis of the Run Ib inclusive jet cross section is shown in Figure 11. It rises from 0.95 to a maximum of 1.19 at $E_T \simeq 90$ GeV, followed by a slow fall to 1.13 at $E_T \simeq 500$ GeV. The error bands shown in Figure 11 correspond to upper and lower excursions of the errors of Table III, summed in quadrature We assume all

TABLE III. Hadronic Energy Scale Errors. Itemizations of bias, offset, cell-level, and showering corrections are given. All errors for the absolute scale are combined here. The row labelled 'cryostat-factor $k_T$' refers to initial state radiation passing down the beampipe.

| Correction/Source of Error | Monte Carlo | Collider Data |
|---|---|---|
| Bias: | | |
| statistical | from fit | from fit |
| binning @ 10 GeV (jet $E_T$) | 5.0 (1.0 NN) | 5.0 |
| " " @ 15 GeV | 0.5 (0.0 NN) | 0.5 |
| $\eta$-dependence @ 10 GeV | 0.0 | 2.0 |
| " " @ 15 GeV | 0.0 | 1.0 |
| Offset: | | |
| statistical | 0.0 | 0.0 |
| underlying event systematic | 0.1/energy | 0.1/energy |
| uranium noise systematic | 0.0 | $0.2/E_T$ |
| Cell-level: | | |
| cryostat-factor statistical (for EC) | 0.0 | 0.48 |
| cryostat-factor mult-interaction " | 0.0 | 2.0 |
| cryostat-factor $k_T$ " | 0.0 | 1.0 |
| high voltage scale (reco<11) | 0.0 | 0.0 |
| non-ICR sampling (reco<12) | 0.0 | 0.25 (ave.) |
| ICR sampling (reco<12) < 40 GeV $E_T$ | 0.0 | 0.0 |
| ICR sampling (reco<12) > 40 GeV $E_T$ | 0.0 | 2.0 |
| Absolute Response: | | |
| statistical | from fit | from fit |
| @ 10 GeV jet energy | 2.29 | 3.95 |
| @ 15 GeV jet energy | 1.50 | 3.55 |
| @ 20 GeV jet energy | 1.19 | 4.07 |
| @ 30 GeV jet energy | 0.00 | 2.77 |
| @ 80 GeV jet energy | 0.00 | 2.00 |
| @ 150 GeV jet energy | 0.88 | 1.82 |
| @ 400 GeV jet energy | 1.43 | 4.23 |
| Showering: | | |
| statistical | 0.0 | 0.0 |
| systematic | 1.0 | 1.0 |

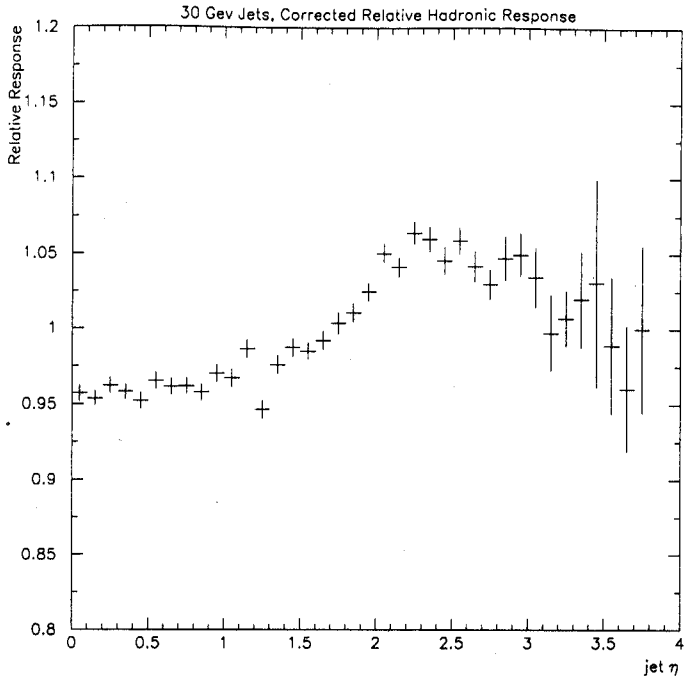


FIG. 12. Relative hadronic response as a function of jet pseudorapidity after the full ICR corrections are applied. The $\eta$ dependence in the ICR region is gone.

systematic errors uncorrelated with each other except in a few cases noted above. There are point-to-point correlations in the systematic errors which can be obtained from Tables I, II and III. An example is the instrumental background in the absolute scale measurement. If we are 1.0% low from this systematic at 50 GeV then we are 1.0% low virtually everywhere. The band as shown indicates an error of about 5% in the energy scale for jets with $E_T \geq 300$ GeV. In several cases, the systematics are believed to be asymmetric in some way; however, we have not attempted to accomodate this in our error analysis so far. The errors are listed in Table III.

## VI. VERIFICATION OF HADRONIC ENERGY CORRECTIONS

With the various correction factors determined, we need to verify that we have achieved our goal of getting to the particle level energy uniformly in pseudorapidity, energy, and $RMS_{\eta,\phi}$. We briefly describe the verification of our two main relative corrections in terms of pseudorapidity and $RMS_{\eta,\phi}$. Then we compare our measured jet response in Data, and Monte Carlo. Lastly, we use $Z + jets$ events to estimate the quality of the corrections in Monte Carlo and Collider Data events.

### A. Cross-checks of Relative Corrections

The largest $\eta$-dependent correction is the ICR correction. We test the effectiveness of this correction by rerunning on a multijet sample with this correction applied. Figure 12

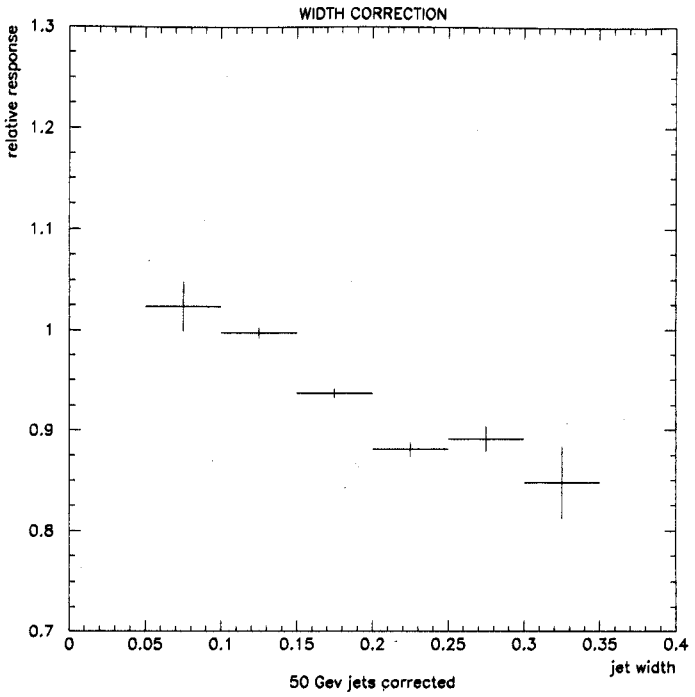


FIG. 13. Relative hadronic response as a function of jet angular width for central jets after the width correction.

shows the measured response vs detector $\eta$ which is now smooth in the ICR region.

Applying the RMS-dependent response correction to a sample of dijet events produces Figure 13. The curve has been signficantly flattened out but not completely. The main reason for this is that we cannot correct unreconstructed energy correlated with the probe jet. A similar analysis of multijet events is nearly flat for this and higher $E_T$ bins.

### B. Cross-checks of Energy Scale using Monte-Carlo

As mentioned above, we have measured the ratio of Monte Carlo and DØ responses to be 1.075. This comparison is misleading, however, because we have corrected the photons in order to properly combine and compare 1a and 1b (see [18]), and we have not corrected the jets by such a factor. What is perhaps more useful is a statement of the inherent response of the calorimeter for jets relative to photons. This is shown in Figure 14 for data and Monte Carlo, and it indicates that the Monte Carlo has predicted our *in situ* measurement to within 2% which is well within our systematic errors. Interestingly, a totally different method has previously been used to predict jet response using testbeam particles input into ISAJET particle jets [23]. Although the errors from such an analysis are quite large, the resulting curve agrees well with the measurements from collider data and Monte Carlo presented here.

An explicit check of the relation between corrected calorimeter jet energy and the matching particle level jet energy has also been attempted. Figure 15b shows the ratio of calorimeter and particle jet energy vs particle jet energy before corrections (open circles) and after corrections (solid circles). The sample used here was a sample of ISAJET direct photon

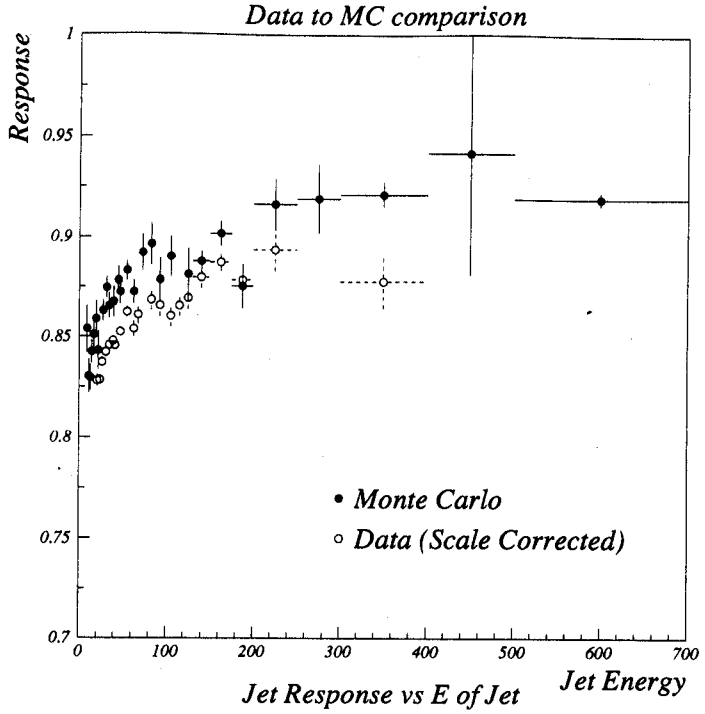


FIG. 14. Response of the probe jet versus mean jet energy for Data (open circles) and Monte Carlo (solid circles). The data has had the EM-scale applied to put the two samples on the same footing (ie. response relative to photon).

events with no cuts on the hadronic recoil. Although the ratio is close to unity after corrections, at very large energies there is a discrepancy between calorimeter and particle jets. On the other hand, the $\not\!\!E_T$ is shown to balance in Figure 15a. A detailed study of this is in progress, but is not yet complete.

### C. Jet and $\not\!\!E_T$ balance in Z Samples

Tests of the hadronic correction were made by looking at events where a Z boson decayed to two electrons. The corrected hadronic response can be determined by looking at the dielectron system and the recoil hadronic system along a fixed direction in space. These systems should exactly balance in an ideal calorimeter. We choose as our fixed direction the angular bisector of the two electrons in the transverse plane. We denote this direction as $\hat{\beta}$. Since these events have presumably no real source of $\not\!\!E_T$, the average component of $\not\!\!E_T$ along $\hat{\beta}$ should be zero.

The plots in Figure 16 show the component of $\not\!\!E_T$ along $\hat{\beta}$ for Z dielectron events with at least one jet. In all plots, the electrons were corrected and these corrections were applied to the $\not\!\!E_T$. For the dashed points, the jet corrections are not applied while for the solid points they are. The top left plot gives the effect in Run 1a, top right is for Run 1b, and the bottom left plot is the projected $\not\!\!E_T$ in HERWIG Z events. It is clear that the corrections remove most of the net $\not\!\!E_T$ along $\hat{\beta}$. However, it should be pointed out that we expect the points to be at zero only when the entire calorimeter has been calibrated. We have only

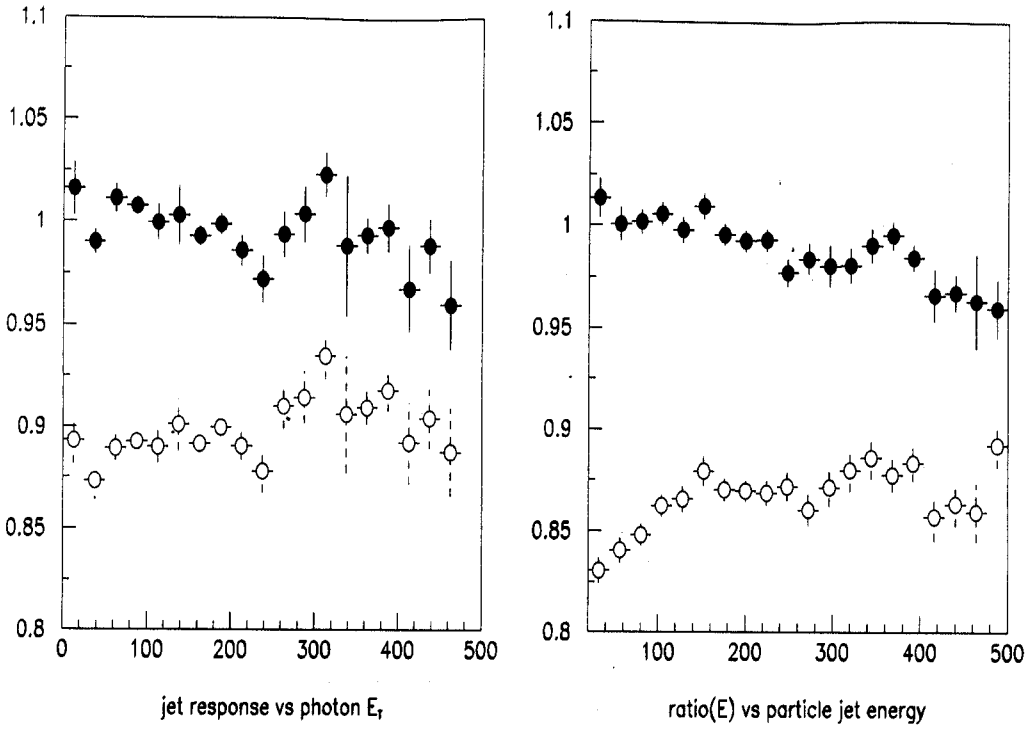


FIG. 15. a) Response of calorimeter vs photon $E_T$ in ISAJET direct photon events is shown after (before) corrections in solid (open) circles. b) Ratio of reconstructed jet energy to particle jet energy vs particle jet energy after (solid circles) and before corrections (open circles).

calibrated jets and electromagnetic showers. Unclustered energy is left uncorrected here.

Figure 17 shows the importance and effect of unclustered energy. This is a similar plot made with Z dielectron events with no found jets. The only thing that can balance the $p_T$ of the Z in these events are the unclustered cells. The less graduated curve is the result of applying soft recoil correction to the vector sum of all the unclustered energy in the calorimeter. It appears to do a reasonable job, although this correction was derived from these same events. Unfortunately, this correction does significantly worsen the $\not\!\!E_T$ resolution [21].

Another potential comparison of our energy scale can come from applying the MPF method to both the photon and Z samples in the same way. An measurement of the average response of the recoil of central photons has been performed using Run 1a data with no restriction on the recoil. The resulting number is in excellent agreement with that obtained from Z events in the W mass analysis (ie. $R = 0.83$) [18,7].

## VII. CONCLUSIONS

We have calibrated jets in the DØ calorimeters to compensate for noise, spectator interactions, response, and showering. The overall correction is between 13% and 19% for 0.7 cone jets above 20 GeV. Our error has been estimated, independently of Monte Carlo and Z verification samples, to be about 5% below 20 GeV and above 300 GeV, and about 2.5% at 80 GeV. The calibration is constrained by data from 20 GeV thru 350 GeV, with

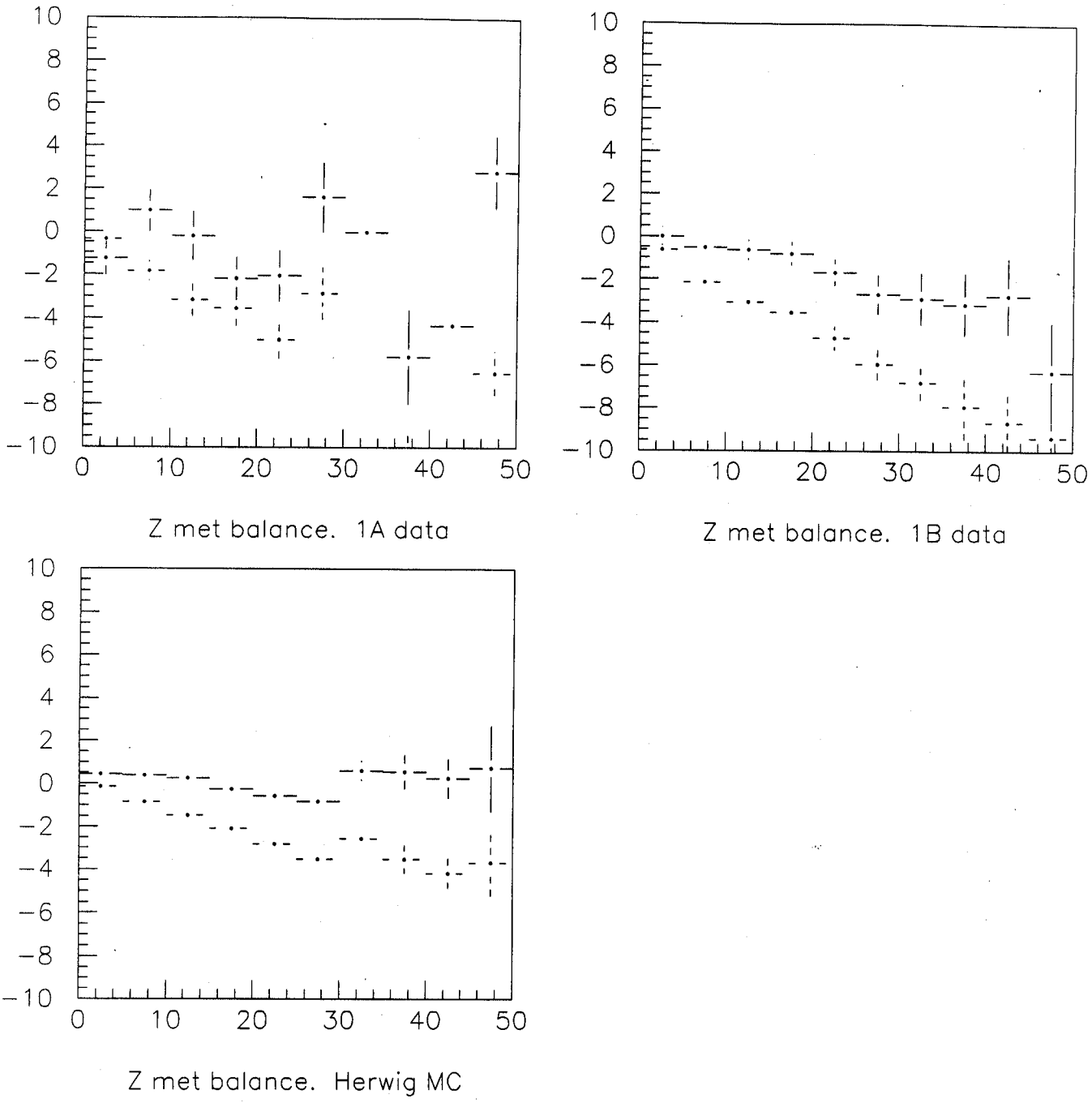


**FIG. 16. The average $\not\!\!E_T$ along the $\hat{\beta}$ direction as a function of $p_T$ of the Z boson along this direction when one jet is present and corrected. The jet correction reduced the imbalance.**

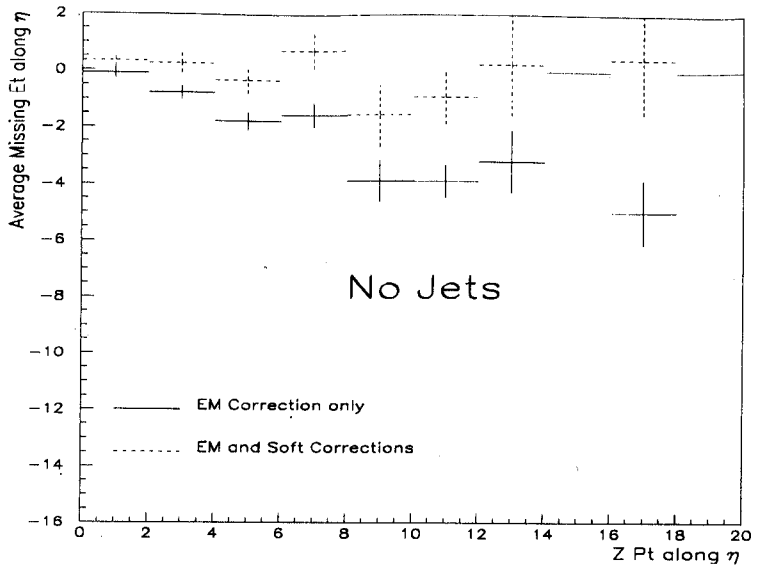


FIG. 17. The average $\not\!\!E_T$ along the $\hat{\beta}$ direction as a function of the $p_T$ of the Z boson along this direction where no jets are present. Corrections to the unclustered energy are effective in removing the average $E_T$ imbalance.

the portion above 150 GeV coming from an EC extrapolation with a modest systematic error. Above 350 GeV and below 20 GeV a Monte Carlo sample is used to make the extrapolation.

Predictions of jet response in the Monte Carlo is in agreement with our measured energy scale in the data within our errors. Additionally, an explicit comparison in Monte Carlo samples of calorimeter and matching particle jet energies indicates we have correctly calculated $E^{jet}_{particle}$ to within our errors. Verification from Z dielectron events, while susceptible to model dependencies, confirms the validity of both scale and error at low $E_T$.

Many people have contributed to these analyses over time and there are many people to thank. In particular, we are glad for Andy Milder's early work which helped serve as a general basis for what has become our energy scale. Also, we are grateful to Harry Weerts for advice and lots of help in this document. Special thanks also go to Linda Coney, Gian Di Loreto, and Brent May for help in various pieces of the correction. We are grateful to Hugh Montgomery for help in documentation and Scott Snyder, Chip Stewart, and Jaehoon Yu have helped in various needed ways.

# REFERENCES


[1] B. Abbott, M. Bhattacharjee, D. Elvira, F. Nang, H. Weerts. "Fixed Cone Jet Definitions in DØ and $R_{sep}$". DØNOTE 2885, 3/96.

[2] DØ Collaboration, S. Abachi et al., "The DØ detector", Nucl. Instrum. Methods Phys. Res. Sect. A338, 185(1994).

[3] DØ Collaboration, A. Aihara et al., Nucl. Instrum. Methods Phys. Res. Sect. A325, 393(1993).
S. Abachi et al., Nucl. Instrum. Methods Phys. Res. Sect. A324, 53(1993).
Joan Guida, "Performance and calibration of the DØ uranium liquid-argon Calorimeter", Proceedings of the 4th International Conference on Advanced Technology and Particle Physics, Como, Italy, October 3-7, 1994, Fermilab-Conf-95/010-E.
John Borders, "Optimization of Jet Energy Resolution and Response of the DØ Detector", PhD. thesis, U. of Rochester, DØNOTE 2219, 4/94.

[4] U. Heintz, 'A Measurement of the Calorimeter Response Using $\pi^0$ Decays', DØNOTE 2268, 8/94.
I. Adam et al., 'Observation of $J/\psi$ to ee decays at DØ and calibration of the central calorimeter electromagnetic energy scale', DØNOTE 2298, 10/94.
S. Rajagopalan, 'An Estimate of the Energy Scale Offset at DØ', DØNOTE 2481, 4/95.

[5] R. Hirosky, "Response of DØ U-LAr Calorimeters at Low Energies and the Effect of Oxygen Contamination on Observed Signals', PhD. thesis, U. of Rochester, 1992.
DØ Collaboration, M. Tartaglia, "The $e/\pi$ and $\pi^0/\pi$ Ratios Measured, and Monochromatic $\gamma$ and $\pi^0$ Beams Explored in the DØ Test Calorimeter", Proceedings of the 3rd International Conference on Advanced Technology and Particle Physics, Como, Italy, June 22-26, 1992, Fermilab-Conf-92/273.

[6] DØ Collaboration, Jon Kotcher, "Design, Performance and Upgrade of the DØ Calorimeter", Proceedings of the 1994 Beijing Calorimetry Symposium, IHEP - Chinese Academy of Sciences, Beijing, China, October 25-27, 1994, pp. 144-158, Fermilab-Conf-95/007-E.

[7] M. Demarteau, J. Sculli, K. Streets, "Measurement of the W-mass", DØNOTE 2929, 4/96.

[8] DØ Collaboration, W. Dharmaratna, "Effect of Dead Materials on Calorimeter Response and Monte Carlo Simulation", Proceedings of the 3rd International Conference on Calorimetry in High Energy Physics, Corpus Christi, Texas, Sep 29 - Oct 2, 1992, Fermilab-Conf-92-309.

[9] Rich Partridge, private communication.

[10] J. Jaques, "Punchthrough in the Central Calorimeter", DØNOTE 2062, 2/94.

[11] Kaushik De, FNALDØ DØNEWS #1277 (General folder).

[12] Chip Stewart, CSF_HV.RCP, 11/92.

[13] Bob Kehoe, 'Resolution Bias in Jet Response Measurement', DØNOTEs 2052 and 2053, 2/94.

[14] CDF Collaboration, F. Abe et al., Fermilab-Pub-92.

[15] Richard Astur, 'Energy Scale Corrections', DØNOTE 2089, 4/94.

[16] Richard Astur, 'On Correcting Jets by Correcting the Electromagnetic and Hadronic Calorimeters Separately', DØNOTE 2575, 5/95.

[17] Meenakshi Narain, private communication.

[18] Bob Kehoe, 'Measurement of the Absolute Hadronic Energy Scale at DØ', DØNOTE 2931, 5/96.
[19] F. Paige and S. Protopopescu, Report No. BNL38034, 1986 (unpublished).
[20] C. Fabjan, Calorimetry in High Energy Physics, in Experimental Techniques in High Energy Physics, Ed. T. Ferbel, Addison-Wesley, 1987.
[21] T. Joffe-Minor, R. Astur, "A Study of the Effects of the CAFIX Energy Scale Corrections, DØNOTE 2211, 7/94
[22] G. Marchesini and B.R. Webber, Nucl. Phys. B310 (1988) 461, version 4.6.
[23] A. Milder, R. Astur, 'Jet Energy Scale using Test Beam Data', DØNOTE 1595, 12/92. DØ Collaboration, Chip Stewart, "Jets in the DØ Calorimeter", Proceedings of the 3rd International Conference on Calorimetry in High Energy Physics, Corpus Christi, Texas, pp. 741, Sep 29 - Oct 2, 1992, DØNOTE 1516.

## APPENDIX A: DETAILS OF OFFSET ANALYSIS

### 1. Underlying Event

The Minimum-Bias trigger only requires hits in the forward and backward hodoscopes with the intention of only accepting events where the proton and antiproton fragmented. The energy distribution of these events is expected to be similar to the contribution from the fragmented proton and antiproton following a hard partonic scattering. This assumption is flawed to the extent that the scattered partons remain color connected to the beam and jets in the event and interact with them. For instance, the energy may be concentrated loosely in the vicinity of the hard interaction jets and therefore not be uniform in $\phi$. Also, the energy may increase when a hard interaction is present which can pull extra energy from the beamline. It has been suggested that this contribution is exactly what should be subtracted.

Using the instantaneous luminosity to determine the number of interactions on average for each event has a Poisson error in the average number. This is bigger than what could be obtained if one determines the correction event by event (through the multiple interaction tool for example). Further, some trigger samples actually make cuts/requirements on the number of interactions making this correction inappropriate in those cases.

It may be noted that in the detector, the particles comprising the underlying event have some finite response, $R_{ue}$, which is likely different than $R_{had}$. Thus, what we call underlying event is really $R_{ue}U$, not $U$. Assuming it is $\phi$ symmetric, however, this is just what we need to subtract from found jets.

### 2. Zero Suppression and Uranium Noise

The output distribution of each calorimeter channel in a quiet detector is referred to as its 'pedestal' distribution and the average of this distribution is referred to as its pedestal. The pedestal of each channel is subtracted during readout which means the noise contribution over time for each channel should be zero. Because finite noise distributions mean that practically all channels (about 48K) have nonzero values, transferring all of this data taxes

both computing power and space. Therefore, each channel is 'zero-suppressed' meaning that if a channel readout is within two standard deviations (as determined from the pedestal distribution) of zero after pedestal subtraction, it is set exactly to zero and not read out. This dramatically reduces the amount of calorimeter data that must be transferred. It should be noted that some amount of real jet energy is lost when the calorimeter is zero suppressed. Effectively, such a loss changes the energy response of the jet so we have chosen to absorb it into $R_{had}$.

Left to itself, electronic noise lends an approximately gaussian output distribution to the various channels in the absence of particles. Because of its symmetric shape, even after zero suppression this noise would contribute no energy to a jet on average. The absorber plates in the fine portions of the DØ calorimeter system, however, are made of depleted uranium whose decay results in electrons being ejected into the active medium and detected. This "Uranium noise" adds positive tails to the pedestal distribution. Because the zero suppression cut is symmetric around the mean, a net positive energy contribution remains from uranium noise. This effect was seen in early module tests and is seen in special runs where there is no beam in the accelerator and only noise is read out. Since DØ has a fairly constant number of channels per pseudorapidity interval we expect the energy contribution to be constant as a function of pseudorapidity which implies that the $E_T$ contribution falls off as $sin\theta$.

### 3. Pileup and Cell Occupancy

A further complication to the offset results from effects which depend on cell occupancy. The total offset in a given cell depends on whether that cell has been exposed to significant energy in the current event, a previous event, or not at all. For instance, as the luminosity increases cells will have higher occupancy from collisions occurring just prior to the current one. This results in a gradual negative slope to the cell energy causing the baseline to be higher before cell readout than during it. This effectively removes energy from the cell and counters at some level the increase in energy from additional interactions. This will have a luminosity dependence and has so far been ignored.

Both $U$ and $N$ are dependent on the number of occupied cells within the jet. It has been estimated [9] that $U$ doubles when all the cells are occupied since zero suppression is effectively turned off. Further, $N$ becomes much smaller in this case because occupied cells are not biased by the zero-suppression cut. One might then argue that these numbers should be adjusted depending on the fraction of cells in the jet that are occupied. However this effect is corrected for on average when the jet scale is anchored to an absolute scale with photon+jet events. This is because the photon is relatively insensitive to this effect causing it to show up in the $\not\!\!E_T$ and thus be calibrated out. Therefore we subtract the full $N$ and $U$ values. However as the cell occupancy increases (due to increased luminosity for example), further corrections would be needed (see below). For events where the jet has a larger occupancy than the sample used to determine the correction an extra adjustement is needed, we expect the jet $E_T$ to be adjusted by:

$$\Delta E_T = \Delta f(\Delta N + \Delta U + \Delta Z) \qquad \text{(A1)}$$

$\Delta f$ is the change in the occupancy of the cells in a jet and the other terms are the change in the respective contributions from noise, underlying event and the energy lost from the

jet due to zero-suppression. $\Delta N$ should have the opposite sign of the other two variables and partially mitigate this effect. As an example, in the very central region, let us assume that zero-suppression causes a loss of 50% of $U$ and a similar reduction in the energy lost from the jet. We would get a change of (-1.64 + 0.310*2 + 0.310 )*.2 = approximately -40 MeV/rad/$\eta$ for an event with two spectator interactions in which the average cell occupancy had increased by 20%.

## APPENDIX B: APPROXIMATE CELL-LEVEL CHANGES FOR DØ RECO VERSION 10/11

In Run 1a at run 52470, the high voltage setting for calorimeter power supplies was reduced from 2.5 kV to 2.0 kV. This produces a shift in response of calorimeter cells which was not compensated for in DØ RECO Version 10. We attempt to correct jets by using the factors given in [12] indicated for reference in Table IV. These corrections are applied to the

TABLE IV. High Voltage cell-level corrections for reconstruction version 12.

| Calorimeter section | CC | EC |
|---|---|---|
| EM | 1.015 | 1.016 |
| HAD | 1.023 | 1.019 |

stored EM and hadronic energy (1.0-EM-ICR) fractions of the jet. Also, one power supply of the calorimeter has been at 1.6 kV (PS 92) rather than 2.0 kV because of an oscillating current. No version of DØ RECO (up to 12.21 at least) has compensated for this and we do not attempt to do so here since the effect is minor.

For DØ RECO version 12, sampling weights were changed for all calorimeter cells from previous reconstructions. These changes are generally constant for all layers in a compartment (ie. all CC FH cells get 5.1% regardless of layer), but EM cells were changed layer-by-layer. Since we have the EM, CH, and (indirectly) FH fractions on the micro-DST, we have determined approximate corrections which average the various actual sampling weight changes by a typical longitudinal jet profile in that compartment. Since only the EM sampling weights changed layer-by-layer, this weighting only affects the EM correction. We ran DØ RECO version 11 and 12 over 400 jets using the nominal vertex (ie. z = 0.0 cm) and obtained histograms of the ratios of the $E_T$ in each compartment (EM, FH, CH) and plotted it vs $\eta$. The ratio is version 12 reconstruction divided by version 11. There is some scatter to the points but the values come out to be as in Table V. As an example of weighting over the four EM layers, a typical CC electron would have gotten a scale factor of about 1.01 in EM energy as opposed to 0.995 for a jet.

In Figure 18 is shown the $\eta$ dependence of measured probe jet response in dijet events in Run 1a. An attempt was made to apply the corrections derived by the ICR group. A difficulty arises because we do not know the cell-by-cell itemization of energy in the jets in the ICR so the correction, while it helps, does not remove all the dependence. Thus, as mentioned above, further parametrizations of these curves were needed to finish the job.

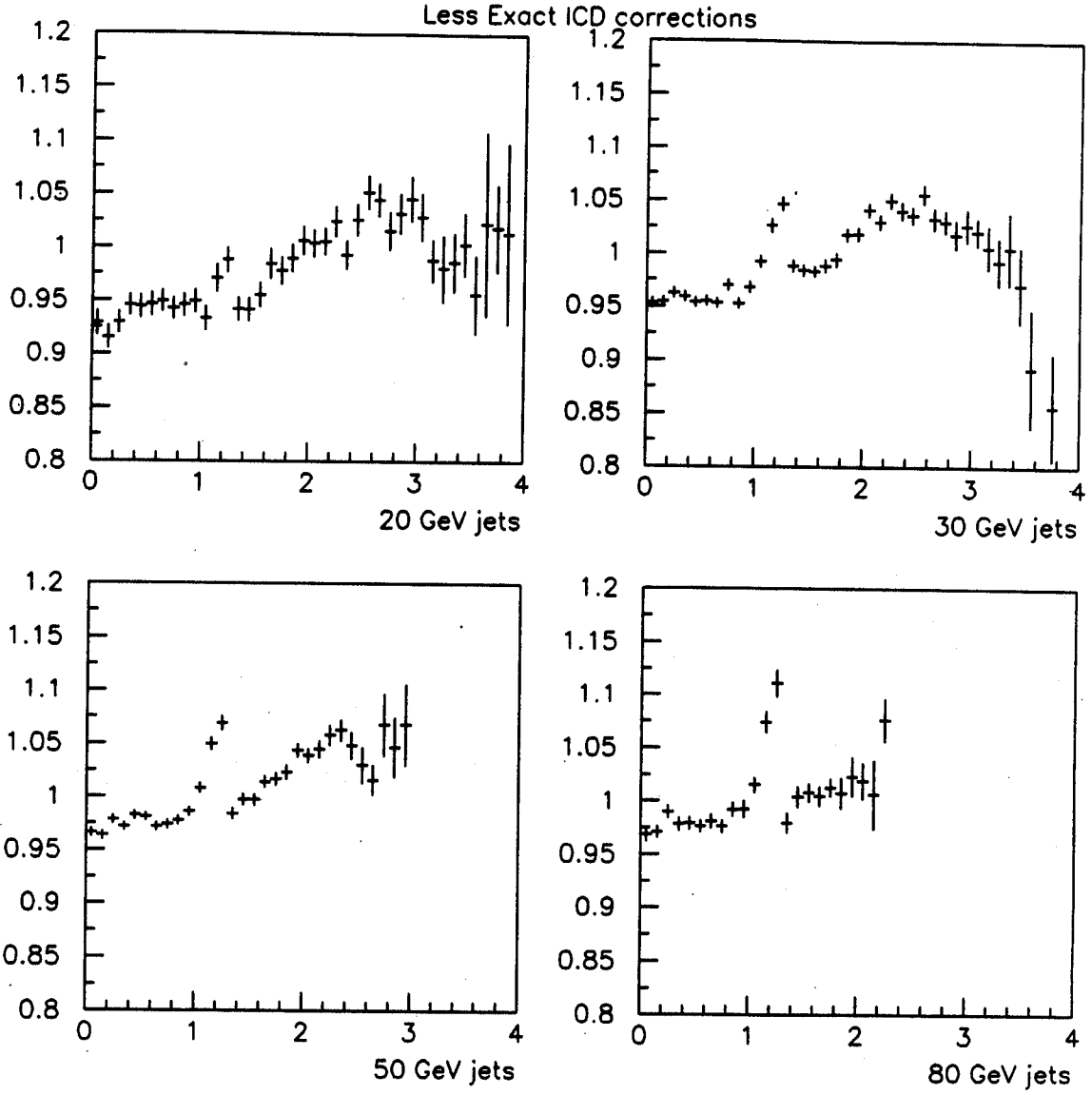


FIG. 18. Relative response vs $\eta$ for Run 1a data with partial corrections. The corrections remove part of the ICR bump, but not all.

TABLE V. Sampling weight changes for calorimeter layers in reconstruction version 12.

| Calorimeter section | CC | EC |
|---|---|---|
| EM | $0.995 \pm 0.005$ | $0.990 \pm 0.002$ |
| FH | $1.051 \pm 0.001$ | $0.980 \pm 0.005$ |
| CH | $1.051 \pm 0.001$ | $0.987 \pm 0.001$ |

An initial estimate of the $\eta$ dependence of jets in Run 1b was attempted using both dijet and direct photon samples. Figure 19 shows the relative response versus probe jet detector $\eta$ in dijet events. The large ICR bump is absent and it appears that a small dip is present in the same region. Given the size of the errors and the dip, a correction for the ICR in DØ RECO 12 has not yet been attempted.

## APPENDIX C: CODE SUMMARY

All of the corrections discussed in this document are performed by individual routines called within the CAFIX package; most operations are performed by calls within QCD_JET_CORRECTION.FOR. This routine is fairly modular and refers to separate Monte Carlo and Collider Data QCD_JET_CORRECTION_RCP files for correction parameters. The code has changed very significantly from CAFIX version 4.2 to 5.0 which this document describes, so the details can only be taken for version 5.0. The general structure of CAFIX is the following:

- Correct all PELC and PPHO clusters with electromagnetic energy scale by calling CORRECTEM.FOR. By default in CAFIX V5.0, all clusters are now corrected instead of just those satisfying an isolation cut as before. This correction is controlled by toggling DO_EM_CORRECTION. If DO_MET_CORRECTION is also on, the EM-scale changes will be propagated into the $\not\!\!E_T$.

- For each jet algorithm, loop over all jets. Any matching PELC or PPHO clusters are removed from each JETS bank by CORRECT_JETS_EM_REMOVE.FOR. Only up to two matching EM-cluster banks are removed currently because the micro-DST only stores two such links. Currently, the PELC or PPHO clusters are removed from the JETS bank vectorially instead of using the JNEP banks. If CORRECT_EM_JETS is toggled on, then the remaining JETS bank energy is corrected by QCD_JET_CORRECTION.FOR.

- Loop over all jets for all jet algorithms and apply the jet corrections by calling QCD_JET_CORRECTION.FOR, and then overwrite the JETS banks with the corrected quantities. Also, the various errors and correction factors are stored in the JETS bank. The following path is followed (if the relevant switches are set in QCD_JET_CORRECTION_RCP):

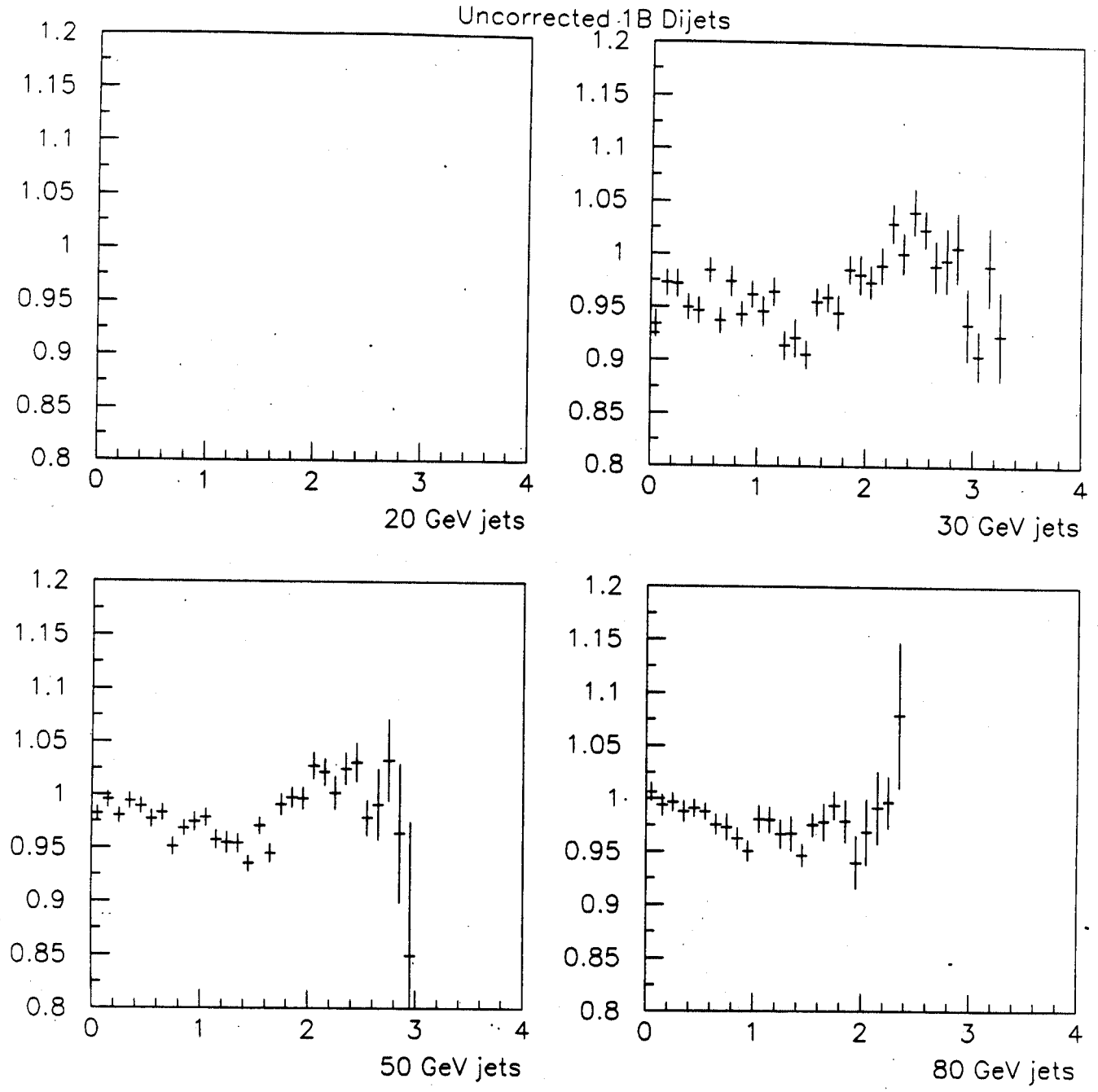


**FIG. 19. Relative response vs $\eta$ for Run 1b data before any corrections. Compared to Run 1a, the response is flat.**

- The bias correction is performed by MPF_LOW_ET_BIAS_CORR.FOR. This is currently only used when measuring later correction factors, in particular the absolute scale. It is controlled by DO_BIAS_CORRECTION in QCD_JET_CORRECTION_RCP and its default setting is off. Thus its errors are read into the absolute scale correction routine, MPF_JETCORR.FOR, as unbiasing errors.
- The offset correction is performed by CORRECT_JETS_NOISEU.FOR. This correction has two pieces: underlying event and noise. One can control both by toggling DO_ZSP_CORRECTION and DO_UND_CORRECTION in CAFIX_RCP, and both are set .TRUE. by default. An example manipulation is for 630 GeV running or Monte Carlo. Once the $E_T$ density in MIN-BIAS events is known (in the functional form =UNDER_A0_DENSITY+UNDER_A1_DENSITY*abs(eta)), they can be simply input into these variables in the RCP file. Another feature of this correction is that one can turn off the luminosity dependence (ie. switch back to using MI_TOOL) by toggling the USE_LUM RCP switch.
- The routine CORRECT_JETS_SCALE_FACTORS.FOR performs the detector scale corrections. This routine currently needs to be turned off for Monte Carlo otherwise a crash will occur in the ICR section of the code. It is toggled by the DO_DET_SCALE_CORRECTION switch in QCD_JET_CORRECTION_RCP.
- The width correction is performed by CORRECT_JETS_WIDTH.FOR and is toggled by DO_WIDTH_CORRECTION in QCD_JET_CORRECTION_RCP.
- The absolute scale correction is applied by MPF_JETCORR.FOR. Since the Collider Data response curve between 120 and 350 GeV is obtained from EC jets, this portion of the curve has an additional systematic error if we are dealing with a central jet in MPF_JETCORR.FOR. The number is read in from the cryostat portion of QCD_JET_CORRECTION_RCP. Also, if the bias correction is turned off then the errors for that correction are interpreted as unbiasing errors for this correction. They are read in by this routine and applied to jets. This correction can be toggled by the switch DO_RESPONSE_CORRECTION in QCD_JET_CORRECTION_RCP.
- The showering correction is applied by CORRECT_JETS_OOC.FOR and is controlled by the DO_CONE_CORRECTION switch in CAFIX_RCP.

- Check that uncorrecting jets gives back the original results.
- Loop over PELC and PPHO bank correction vectors and apply them to the $\not\!\!E_T$. Loop again over the $R = 0.7$ cone algorithm and apply its response corrections to the $\not\!\!E_T$. These $\not\!\!E_T$ corrections are turned off by toggling DO_MET_CORRECTION in CAFIX_RCP.
- Loop over PMUO and add those passing a quality mask into muon-included $\not\!\!E_T$ (PNUT(5)). The quality mask is GOOD_MUON_MASK in CAFIX_RCP.
- Apply soft recoil correction to $\not\!\!E_T$ if requested (DO_SOFT_CORRECTION = .TRUE.).